Effect of Injection Dynamics on Wave Propagation in a Linear Detonation Combustor

Aaron Lemcherfi[a], Rohan M. Gejji[a], Zach M. Ayers[b], Ethan W. Plaehn[a], H. Douglas Perkins[d], Terrence R. Meyer[a,b], Sukesh Roy[c], Christopher Fugger[c,*], and Carson D. Slabaugh[a]

[a] *School of Aeronautics & Astronautics, Purdue University, West Lafayette, IN 47907, USA*
[b] *School of Mechanical Engineering, Purdue University, West Lafayette, IN 47907, USA*
[c] *Spectral Energies LLC, Beavercreek, OH 45430, USA*
[d] *NASA Glenn research Center, Cleveland, OH 44135, USA*

Abstract

Injector response to self-excited and sustained detonation wave propagation in an optically-accessible non-premixed natural gas-oxygen linear detonation combustor is investigated. 100 kHz measurements of planar laser induced fluorescence (PLIF) of trace quantities of acetone injected into the fuel supply and simultaneous OH^* chemiluminescence measurements were used to correlate the effect on injection dynamics on detonation wave structure and propagation. Measurements over a range of equivalence ratios (0.61-1.48) revealed wave propagation through regions of high fuel stratification in the axial and transverse direction of reactant injection. Consequently, the propagation of the detonation wave along the channel is through a flow-field with significant variation in fuel mass fraction, reactivity, and sound speeds. At lean conditions, wave propagation frequency is generally lower ($\sim$6 kHz) resulting in longer time between wave passages for mixing and pre-heat resulting in steeper detonation wave-fronts anchored near the injector exit plane. Conversely, at rich equivalence ratios the wave frequency is higher ($\sim$10 kHz) resulting in shorter intra-cycle period for reactant fill and mixing resulting waves lifted from the injection plane that are more compact. Higher chemiluminescence intensity in the post-wave region with deflagrative combustion is observed in these cases. Phase averaged representation of the acetone-PLIF measurements indicate that the fraction of time between wave passages available for reactant fill, mixing and pre-heat is consistent across all equivalence ratios.

Keywords: Linear detonation combustor; rotating detonation engine; rotating detonation combustor; planar laser-induced fluorescence; OH* chemiluminescence

1. Introduction

Rotating detonation engines (RDEs) predominantly operate with non-premixed propellant injection where the dynamic response of the injector to the detonation wavefront is intimately tied to its operability and performance. Periodic reduction or stoppage in reactant flow immediately following detonation wave passage at the injection site followed by the refill process plays a key role on combustor operation. An inadequate reactant refill can starve the wave of fresh reactants resulting in wave-speed reduction and eventual decay. On the other hand, large refill times can result in deflagrative consumption of pockets of premixed reactants before wave arrival, reducing the pressure gain potential of the device [1–3]. While operability and performance of RDEs across a range of operating conditions, propellant combinations, and injector configurations have been studied, detailed characterization of injector dynamics has seldom been reported in experimental studies. In the current work, spatiotemporal evolution of the fuel jet in the combustion chamber and its effect of wave propagation is quantified with high-speed planar laser induced fluorescence (PLIF) of an acetone tracer in the fuel stream and OH^* chemiluminescence measurements in the combustion chamber.

Failure of the injection scheme to deliver homogenized supplies of reactants to the combustion chamber results in localized irregular cellular detonation wave structures [4, 5]. Honhar et al. [6] have shown that a partial decoupling of heat release from the leading shock can result due to detonation wave propagation through sufficiently steep reactivity gradients and can lead to a quenching of the detonation wave front. Conversely, if reactant injection and mixing processes occur too quickly, within the auto-ignition time delay for the reactants, pre-ignition can occur prior to detonation wave arrival [1, 2]. The resultant partial consumption of reactants through deflagration reduces the performance potential of the RDE and can even prevent the generation of stable limit-cycle detonation wave dynamics under certain operating conditions [7]. These findings suggest that a delicate balance between reactant injection and mixing processes relative to the detonation wave circumscription frequency, set by combustor geometry and reactant kinetics, is necessary for optimal combustor operation.

Optical access to the combustion environment provides an avenue for the detailed characterization of wave structure and its impact of combustor performance and operation using imaging and laser-based diagnostics. This data is critical for verification and validation of computational models, which are essential for developing practically applicable RDEs. Curvature of RDE geometries makes optical access and application of detailed diagnostics challenging and only a few studies have reported successful measurements in such devices [8–10]. To alleviate this challenge, an optically-accessible linear detonation combustor that shows multi-kHz self excited detonation wave generation is used in the current work. The mixing and heat-release distribution was simultaneously measured at 100 kHz using acetone-PLIF imaging of acetone as a tracer in the fuel supply and OH^* chemiluminescence respectively.

2. Experiment Description

An optically-accessible linear detonation combustor shown in Figure 1 that promotes multi-kHz self-excited sustained detonation waves was used in this study [2]. Gaseous oxygen was injected axially ($+X$) through a 0.76 mm wide slot spanning the transverse (Y) length of the combustor. Natural gas was introduced at 30° relative to the $+X$ direction through 1.27 mm orifices distributed on alternating sides along the length of the oxidizer slot. Influence of combustion dynamics on the reactant feed system were isolated using sonic orifices installed at the entrance of each reactant manifold. Combustion products were exhausted downstream through axial (X = 90 mm) and transverse (Y = 610 mm) exit boundaries.

Reactant mass flow rates are metered upstream of each manifold with critical flow venturi nozzles. An array of flush-mounted piezoelectric (PCB 113B26) dynamic pressure transducers were used to record pressure fluctuation amplitude in the chamber and reactant manifolds at 2 MHz. Fused quartz windows were installed on either side of the chamber in the Window B region. Chemiluminescence images from electronically excited hydroxyl radicals (OH^*) obtained at 100 kHz at the center (XY) plane in Window B were used to provide a qualitative path-integrated representation of heat-release in the combustion chamber. An UV filter centered at 320 nm with a 40 nm bandwidth was used to isolate background light from the OH^* chemiluminescence (OH^*-CL) signal. The signal was collected with a 98 mm focal-length, f/2.8 objective lens (Cerco Sodern Type-2178), then amplified by a Lambert HiCATT 25 intensifier, and recorded with a Phantom v2512 CMOS camera. The field of view (FoV) for this measurements is highlighted (green box) in Figure 1.

Along with OH^*-CL, simultaneous 100 kHz PLIF measurements of acetone (C_3H_6O) seeded into the fuel supply were acquired to characterize fuel injection dynamics[11]. Liquid acetone flowrate was metered with a cavitating venturi and injected into the natural gas supply pre-heated in a pebble-bed to 400 K to ensure gas-phase injection of the fuel to the experiment. An acetone mass fraction of 10% in the fuel flow stream was used for all tests. Frequency quadrupled Nd:YAG output of a burst-mode laser (Spectral Energies, Quasimodo) was used to generate 12 ns pulsewidth 266 nm pulses for acetone fluorescence excitation. C_3H_6O-PLIF measurements were performed in two configurations. For measurements in the center XY plane, 150 pulses from a laser burst width of 1.5 ms at an average pulse energy of 17 mJ were used to maximize signal to background chemiluminescence intensity ratio. In the second configuration, measurements at six equally spaced horizontal cross planes (YZ) were made, ranging from X=3.2

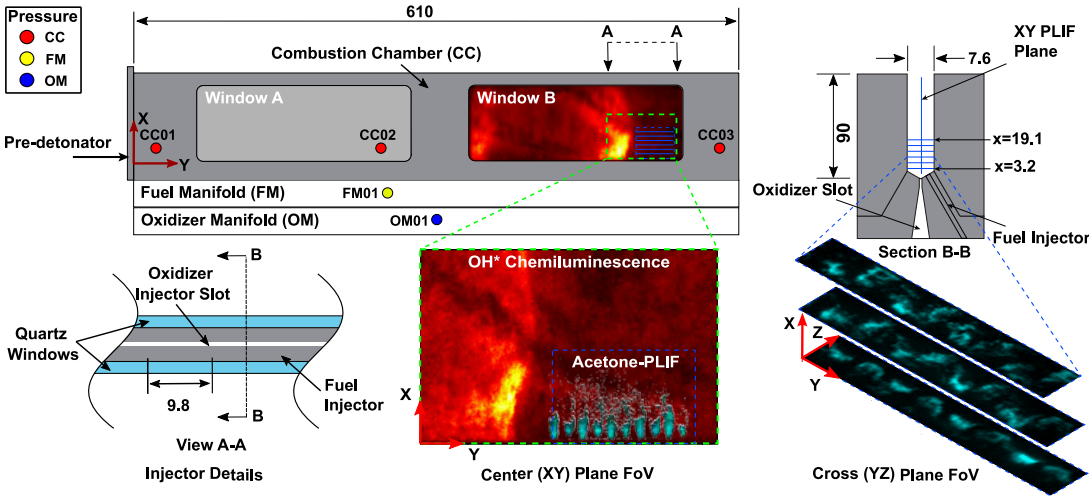

Fig. 1: Schematic representation of the linear detonation combustor. All dimensions in mm.

mm to 19.1 mm. For these measurements, a 50/50 beamsplitter was used upstream of the final turning mirror to produce two parallel 8 mm wide laser sheets with a 12.7 mm spacing in the X-direction. The detection optics and the camera were elevated above the combustor to view both horizontal planes in the same FoV. The X-positions of the final turning optics and of the camera and intensifier were set using synchronized translation stages. This allowed measurements in several planes in consecutive tests while maintaining the Y- and Z-coordinates of the FoV. This configuration provided a spatial resolution of 140 μm/pixel in the Z-direction and 150 μm/pixel in the Y-direction after the images were deskewed in post-processing. For this configuration, 250 pulses with a laser burst width of 2.5 ms at an average pulse energy of 8.3 mJ was achieved. A Phantom v2012 high-speed CMOS camera was coupled to a high-speed Lambert HiCatt intensifier (GaAsP) and equipped with a Nikon 200 mm f/8 visible lens for acetone-PLIF imaging. A bandpass filter (Semrock FF01-439/154) along with a 266 nm longpass filter (Edmund Optics #12-255) were used to isolate the acetone fluorescence, eliminate flame luminosity, and remove spurious scattered laser light from the images. The intensifier gate was set to 20 ns. The FoV was positioned 20 mm from the $+Y$ edge of window B to minimize laser attenuation between the open end of the chamber and the FoV and to ensure that the detonation waves passing through the FoV were fully developed.

3. Results and Discussion

3.1. Combustor Operation

Pressure time history for a representative test, recorded at CC03 highligting steep fronted wave behavior is shown in Figure 2(a-b). A short transient follows ignition at time t=0 s after which limit-cycle dynamics are achieved in the experiment. OH^*-CL measurements are obtained over the entire test duration (∼250 ms) while C_3H_6O-PLIF images are recorded after stationary dynamics are generated in the combustor. Addition of acetone to the fuel supply resulted in an insignificant change in combustor operation or wave dynamics (∼1% change in wave speed(v_{wave})). A detonation surface plot representing a vertically binned OH^*-CL intensity time series is shown in Fig. 2(c) to illustrate the periodic self-sustained wave generation process. Each line of high intensity signal represents propagation of a detonation wave along the length of the FoV while its slope represents wave-speed. The injector response to wave dynamics for seven test cases at a reactant mass flux of 120 $kg/(m^2.s)$ and varying equivalence ratios are presented in the current work. A summary of the test cases is provided in Table 1.

Table 1: Summary of operating conditions.

Case	ϕ	f_{LC} [kHz]	v_{wave} [m/s]	p' [kPa]
A	0.61	6.44	1338	194
B	0.83	6.62	1399	285
C	0.90	8.56	1483	310
D	0.96	10.60	1423	298
E	1.09	10.65	1349	278
F	1.26	10.60	1235	244
G	1.48	10.60	1189	226

3.2. Instantaneous OH^* Chemiluminescence and C_3H_6O-PLIF Measurements

A time series of OH^*-CL and C_3H_6O-PLIF mea-

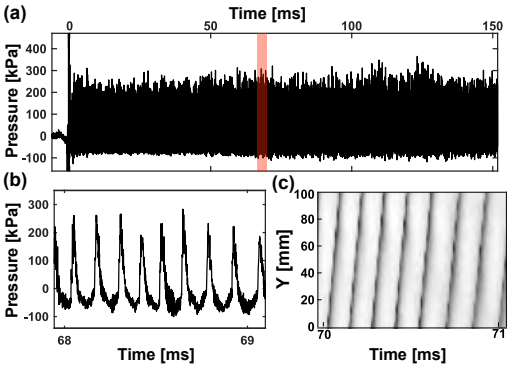

Fig. 2: (a) Pressure fluctuation amplitude (CC03) measured in test Case C (Φ = 0.90) along with a (b) magnified view.(c) Vertically summed OH* chemiluminescence intensity in the Window B region measured during limit-cycle combustor operation.

surements for a lean (Case C ϕ:0.90) and rich (Case F ϕ:1.26) equivalence ratio are shown in Figure 3. For both tests, the sequence of images depict the passage of a single detonation wave through the respective interrogation windows. The C_3H_6O-PLIF FoV extends across ten fuel injection sites. For optimal viewing, both measurements were normalized by their respective peak signal intensities recorded in each frame.

The cycle starts with the detonation wave front represented by the high intensity OH*-CL signal at the edge of the FoV. At this instant in time, the fuel jets have completely recovered from the previous wave passage and are approximately at their maximum fill heights. For Case C and Case F this corresponds to approximately 30 mm and 15 mm respectively. The lower wave frequency corresponding to the lean equivalence ratio case results in a longer fuel recovery time and consequently larger fill height. The fuel jets entering the measurement plane from behind the oxidizer sheet intersect with it $\sim$3 mm downstream of the point of injection and appear displaced from the injector face. The compact jet structure and high signal intensity near the injector face indicates that fuel and oxidizer are not well-mixed close to the injector. As the fuel jets interact with the oxidizer and are heated by combustion products from the previous wave, the signal intensity reduces at downstream locations. The lower fuel refill height at the rich equivalence ratio, despite the higher fuel flow-rate is an indication of unburnt fuel left over after the passage of the previous wave burning in this region increasing local temperature and reducing the PLIF signal intensity.

As the detonation wave approaches the detonation wave-front, represented by the region of high chemiluminescence intensity, high PLIF intensity is observed at the wave-front followed by its rapid consumption in that location as seen at 48.82-48.84 ms in 3(a). The high PLIF intensity at the wavefront (48.83-48.85 ms) suggests presence of locally fuel rich regions that are not fully consumed at the detonation front. The non-premixed injection scheme in the configuration also results in highly stratified local flow, where some of the fuel might be displaced into the PLIF measurement plane with the wave propagating around it, resulting in locally high signal intensity. A fraction of this signal could also be on account of broadband chemiluminescence intensity at the detonation wavefront being recorded in these images. Following the passage of the wave, the fuel PLIF intensity rapidly decreases with near complete extinction observed in 48.85 ms. This is due to the adverse pressure gradient at the fuel injection site from the increase in pressure at the detonation wave front ($\geq$310 kPa). After this time, the fuel jets slowly recover in the time available till the next wave-front arrives and the cycle is repeated.

Similar fuel jet recovery and wave dynamics are observed for the fuel rich Case F shown in 3 (b). Key differences in both the detonation wavefront and the structure of the fuel jets can however be observed between the two cases. For both cases, the wave-front has a forward ($+Y$) lean and extends axially from the injector surface (X = 0 mm) to $\sim$30 mm beyond which an oblique shock is seen. A presence of appreciable amount of OH*-CL signal in the region immediately behind the detonation wave-front at all X locations is observed. This region is indicative of deflagrative consumption of reactants not processed by the wave between successive wave passages. The presence of combustion products in the region closest to the injector surface helps preheat the fresh reactants and prepares them for the arrival of the next wave. On the other hand, this also indicates that not all reactants are consumed in the detonation wave resulting in sub-CJ wave (v_{wave}/D_{CJ} : $70-80\%$ velocities observed in these tests. This is observed to a lesser (lean ϕ) or greater extent (rich ϕ) in all test cases. Evidence of combustion in this reactant refill region is also evident in the C_3H_6O-PLIF measurements that represent the fuel jet injection into the chamber at the center XY plane.

3.3. Phase Averaged Analysis of Heat Release and Fuel Injection Dynamics

Phase averaged images of the OH* chemiluminescence signal are presented for Cases B, C, E, and F are shown in Figure 5. For the phase averaging analysis, the images were discretized into 50 vertical columns and then binned based on the position of the column relative to the instantaneous location of the wave. Binned column images were then averaged and arranged based on phase angle to produce Fig. 5. Phase angles were defined relative to a fixed location just ahead of the wave, arbitrarily set to correspond to 0 degrees. A 360 degree phase interval is used to represent a full detonation wave cycle. A comparison between cases at distinct equivalence ratios indicate a change in wave front structure, with more vertical and distributed heat release distribution observed at lean equivalence ratios followed by for-

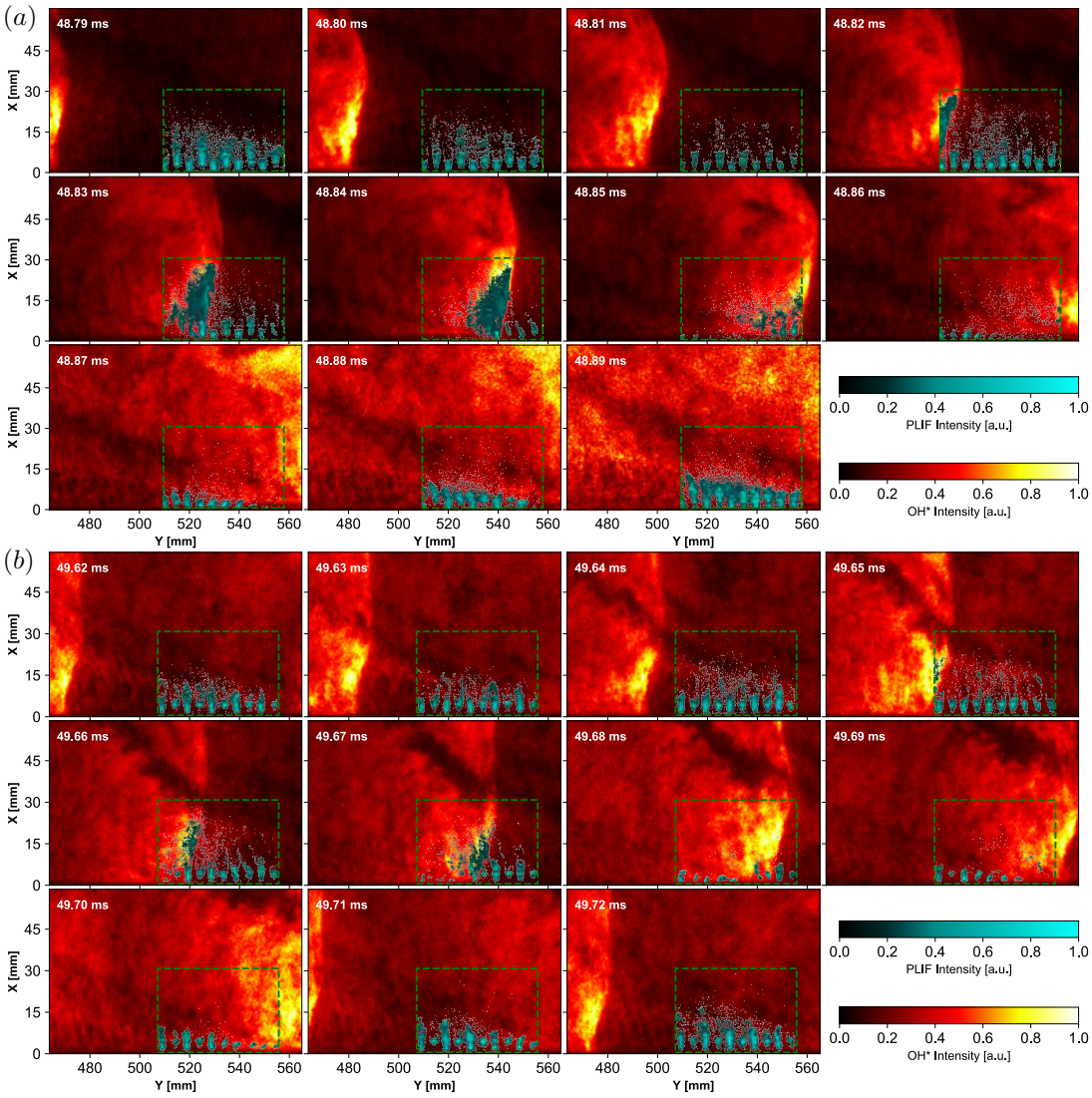

Fig. 3: Time series of OH^* chemiluminescence and C_3H_6O-PLIF signal intensity collected during (a) Case C (Φ = 0.90) and (b) Case F (Φ = 1.26) combustor operation.

ward leaning and compact heat release distribution at ϕ=1.09 and 1.26. The oblique shock and the slip-line downstream of the wave are clearly observed. For each test case, some chemiluminescence intensity is observed behind the wave-front, at higher intensity at richer equivalence ratios. This corresponds to deflagrative combustion behind the wave of reactants not consumed by the wave. Heat release is present in both the post-detonation products from the prior cycle as well as in the reactant refill zone, with sufficient unburned fuel and oxygen present in these zones to support the continued propagation of the detonation wave. Additional measurements are needed to quantify the fraction of fuel consumed in this deflagrative mode.

To compare the phase averaged heat release distribution with fuel distribution in the channel, the phase averaged results for multiple cases are shown in Figure 5. The intensity in the region represented between the blue lines for both PLIF and chemiluminescence images are summed in their vertical bins to obtain line plots showing chemiluminescence and PLIF recovery. A key observation is that the total time available for fuel recovery is invariant as a fraction of wave period for all cases. Fuel recovery time for all cases is shown in Figure 6. The values are obtained

Figure 7 presents phase averaged acetone-PLIF signal intensity obtained during Case B and Case

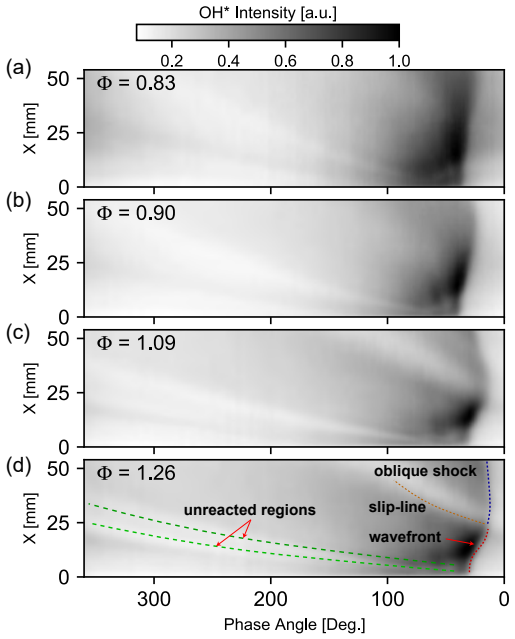

Fig. 4: Phase averaged OH* chemiluminescence measurements for (a) Case B (Φ = 0.83), (b) Case C (Φ = 0.90), (c) Case E (Φ = 1.09), and (d) Case F (Φ = 1.26) combustor operation.

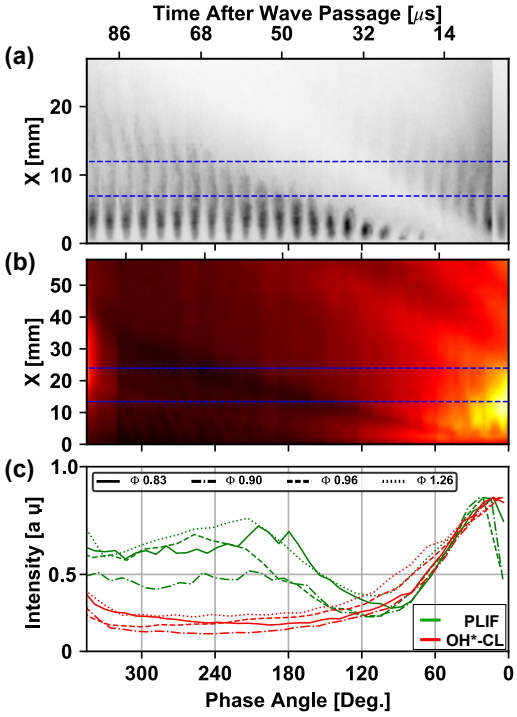

Fig. 5: (a) Phase averaged acetone-PLIF signal and (b) OH* chemiluminescence signal obtained during Case D. (c) Summation of phase averaged acetone-PLIF and OH* chemiluminescence signal obtained between X = 7 mm to 12 mm for Case B, C, D, and F

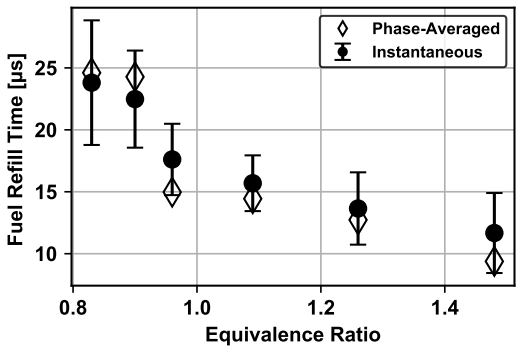

Fig. 6: Fuel recovery time between wave passages using instantaneous and phase averaged acetone-PLIF measurements.

F combustor operation at various cross-plane FOVs. The axial distance between each FOV and the injection surface is provided in the top right corner of each image. High concentrations of acetone-PLIF signal are denoted with higher grayscale (white) color values in this analysis. Fuel injector locations are given by the blue translucent circles shown in the FOV located closest to the injection surface. Wave propagation in Fig. 7 is in the left to right direction. A phase angle of 0 degrees in this analysis corresponds to the leading edge of the wave. The relative difference in convective times required for fuel jets to reach each axial measurement plane during the reactant refill process is denoted with vertical red dashed lines in Fig. 7. The low intensity region downstream (to the right) of the these lines represents regions of hot product gases and residual fuel, existing above the acetone-decomposition temperature, behind the wave.

Initial fuel jet interaction with the oxidizer sheet occurs just below the X = 3.2 mm acetone-PLIF FOV provided in Fig. 7. As fuel from each injection site mixes with the oxidizer sheet and convects axially (X-direction) downstream, an anfractuous fuel distribution is observed. Near the upper bounds of the reactant refill region, this profile diminishes due to interaction between fresh reactants and hot product gases from the previous wave cycle. This is evident in Fig. 7 at FOVs located 22.2 mm and higher above the injection surface.

The trajectory of unreacted fuel in the combustion chamber is visualized by tracking acetone-PLIF signal intensity across each axial FOV in Fig. 7. By examining the axial distribution of acetone for a single phase angle, we can track the fuel supply delivered by a single fuel injector. This analysis indicates that unreacted fuel supplies remain on the same (Z-direction) side of the combustion chamber as they were injected from. Transverse-path integrated mea-

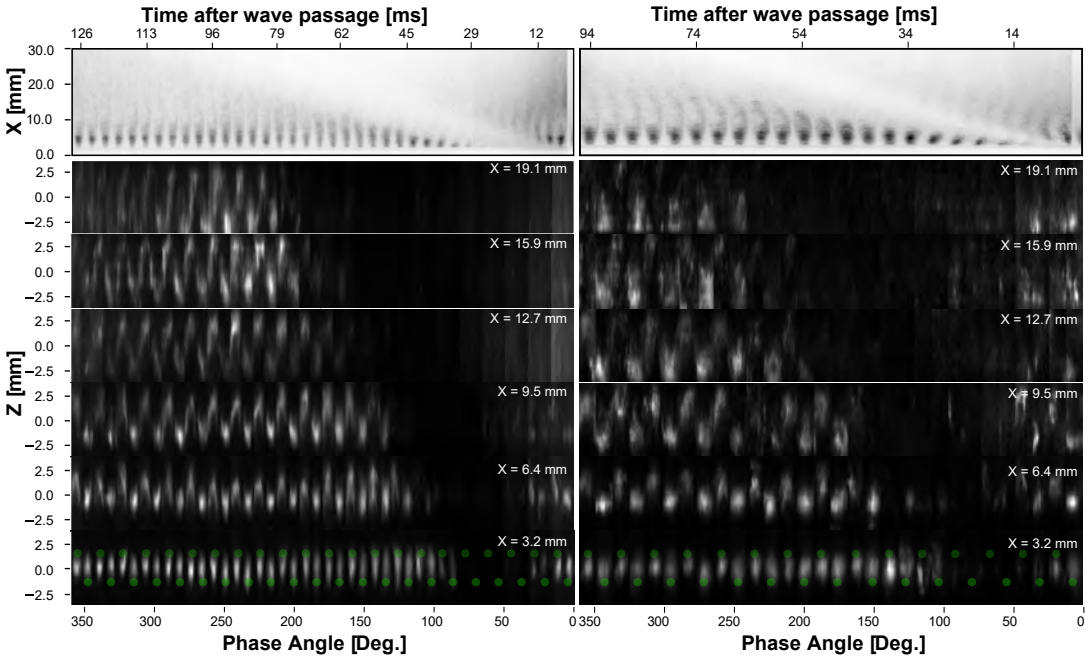

Fig. 7: Phase averaged acetone-PLIF measurements at the vertical center-plane (top) and at varying axial (X-direction) locations over a representative detonation wave period for Case Case B (Φ = 0.83) (left) and Case F(Φ = 1.26) (right). Green dots indicate fuel injection locations.

surements of OH* chemiluminescence provide evidence of deflagration-based combustion in axially-aligned regions just above fuel injection sites. A significant reduction in acetone-PLIF signal due to acetone decomposition is expected within and near heat release regions. These findings require that portions of the fuel jet with highest transverse direction momentum penetrate through the oxidizer sheet (centered at Z = 0 mm). Conversely, the outer edges of each fuel jet, with lower transverse momentum, are unable to penetrate through the oxidizer sheet. This portion of the fuel supply remains unreacted as it mixes with the oxidizer supply and convects axially downstream and toward the side of the combustion chamber it was injected from. The detonability of this reactant supply increases due to induced heating resulting from mixing of product gases from the side of the chamber undergoing deflagration-based combustion. Figure 7 implies that non-premixed injection schemes can result in the generation of highly three dimensional, stratified reactant mixtures. These mixtures are shown here to vary both in reactant temperature and in stoichiometry due to reactant vitiation within the refill region.

4. Conclusion

Response of reactant injection to detonation wave propagation was investigated in an optically accessible linear detonation combustor with 100 kHz simultaneous OH* chemiluminescence and PLIF measurements with an acetone tracer in the fuel stream. The acetone-PLIF measurements were performed in two configurations, one along the center XY plane of the combustor and a second along six YZ planes distributed between X= 3.2 mm $-$ 19.1 mm locations. Simultaneous measurements of heat release and fuel distribution provided key insight into the convolved relation between injection dynamics and detonation wave propagation that can be used the design of optimal injector designs, in linear and rotating detonation wave combustors.

(i) For both lean and rich equivalence ratios, significant spatial variation in fuel distribution is present in the YZ-plane. The detonation wave propagates through a highly stratified mixture of reactants and products along the length of the channel, in the axial and transverse direction. This makes comparison of wave-speeds measured in the experiment with CJ values based on reactant composition tenuous.

(ii) The OH* chemiluminescence images indicate presence of regions of parasitic deflagrative combustion after the passage of the detonation wave. Correlating this with the fuel refill process, there is a clear indication of heat release during the reactant fill and in the post-detonation combustion products from the passage of the prior wave. The pre-heat and partial consumption of fresh reactants prepares them

for the arrival of the new wave which is observed to be critical for self-excited and sustained wave propagation in the linear detonation combustor.

(iii) Phase averaged representation of the heat-release distribution at the wave frequency shows clear distinction in the detonation wave structure between lean and rich test cases. At lean cases, the wave is anchored near the injector surface and extends $\sim$30 mm from it. At rich equivalence ratios > 1.2, the wave has a significant forward lean and the heat release extent in the axial direction is shortened. The locally rich regions at the injector surface also result in the wave being lifted off from the injector surface.

(iv) A mismatch in the fuel and oxidizer injector recovery time was identified using overlaid images of the fuel distribution and heat release fields. This mismatch resulted in significant local variations in mixture composition. The pockets of lean or rich regions were unevenly process by the wave and is a source of inefficient combustion in the experiment.

(v) Fuel flow into the combustion chamber is periodically checked off by the inverse pressure gradient across the injection site after detonation wave passage. The fuel recovery time varies with equivalence ratio (and injector pressure ratio). However, this fuel recovery time is approximately a constant fraction ($\sim 20\%$) of the wave period for all test cases.

Acknowledgments

This work was funded by NASA under Phase I STTR contract 80NSSC19C0551. The high-speed imaging equipment used in this work was purchased with DURIP grant FA9550-16-1-0534 (Program Officer: Dr. Chiping Li) and Defense Threat Reduction Agency Award No. HDTRA1-17-1-0031 (Dr. Jeffery Davis, Program Manager). Ethan Plaehn acknowledges the National Science Foundation for support under the Graduate Research Fellowship Program (Grant DGE-1842166).

References

[1] T. Sato, F. Chacon, L. White, V. Raman, Mixing and detonation structure in a rotating detonation engine with an axial air inlet 000 (2020) 1–8. doi:10.1016/j.proci.2020.06.283.

[2] K. Schwinn, R. Gejji, B. Kan, S. Sardeshmukh, S. Heister, C. D. Slabaugh, Self-sustained, high-frequency detonation wave generation in a semi-bounded channel, Combustion and Flame 193 (2018) 384–396. doi:10.1016/j.combustflame.2018.03.022.

[3] I. V. Walters, C. Journell, A. I. Lemcherfi, R. Gejji, S. D. Heister, C. D. Slabaugh, Performance Characterization of a Natural Gas-Air Rotating Detonation Engine at Elevated Pressure. arXiv:https://arc.aiaa.org/doi/pdf/10.2514/6.2019-4214, doi:10.2514/6.2019-4214.

[4] D. A. Kessler, V. N. Gamezo, E. S. Oran, Gas-phase detonation propagation in mixture omposition gradients, Philosophical Transactions of the Royal Society A: Mathematical, Physical and Engineering Sciences 370 (1960) (2012) 567–596. doi:10.1098/rsta.2011.0342.

[5] S. Prakash, R. Fiévet, V. Raman, J. Burr, K. H. Yu, Analysis of the Detonation Wave Structure in a Linearized Rotating Detonation Engine, AIAA Journal (2019) 1–15doi:10.2514/1.j058156.

[6] Role of reactivity gradients in the survival, decay and reignition of methane-air detonations in large channels, Combustion and Flame 222 (2020) 152–169.

[7] D. P. Stechmann, S. Sardeshmukh, S. D. Heister, K. Mikoshiba, Role of Ignition Delay in Rotating Detonation Engine Performance and Operability, Journal of Propulsion and Power 35 (1) (2019) 125–140. doi:10.2514/1.b37117.

[8] I. V. Walters, R. M. Gejji, S. D. Heister, C. D. Slabaugh, Flow and performance analysis of a natural gas-air rotating detonation engine with high-speed velocimetry, Combust. Flame 232 (2021) 111549.

[9] B. A. Rankin, D. R. Richardson, A. W. Caswell, A. G. Naples, J. L. Hoke, F. R. Schauer, Chemiluminescence imaging of an optically accessible non-premixed rotating detonation engine, Combustion and Flame 176 (2017) 12–22. doi:10.1016/j.combustflame.2016.09.020.

[10] P. S. Hsu, M. N. Slipchenko, N. Jiang, C. A. Fugger, A. M. Webb, V. Athmanathan, T. R. Meyer, S. Roy, Megahertz-rate oh planar laser-induced fluorescence imaging in a rotating detonation combustor, Opt. Lett. 45 (20) (2020) 5776–5779. doi:10.1364/OL.403199.

[11] Z. Ayers, A. Lemcherfi, E. Plaehn, C. Slabaugh, T. Meyer, C. Fugger, S. Roy, Application of 100 kHz Acetone-PLIF for the Investigation of Mixing Dynamics in a Self-excited Linear Detonation Channel, AIAA Scitech 2021 Forum (2021).